Robust Resilience Enhancement by EV Charging Infrastructure Planning in Coupled Power Distribution and Transportation Systems

Jianfeng Wen, *Student Member, IEEE,* Wei Gan, *Member, IEEE,* Chia-Chi Chu, *Senior Member, IEEE,* Lin Jiang, *Member, IEEE,* Jiajie Luo

***Abstract*—Due to the recent rapid developments in fast charging technology for electric vehicles (EVs), these flexible mobile storage resources can provide auxiliary services to the power grid in emergency circumstances. Therefore, it is imperative to develop a resilient enhancement planning scheme for this coupled network under severe contingencies. To this end, this paper investigates a novel robust resilient enhancement scheme for planning charging infrastructure in coupled networks. The objective is to minimize both (i) the investment and operation cost of the coupled network under uncertain traffic demands, and (ii) the EV participation cost for the grid support scheme during contingencies. The investment scheme for power distribution lines and charging stations is determined before the uncertainty realization in the first stage, while the objective function is minimized in the worst possible manner within a specified uncertainty set in the second stage. The nested column-and-constraint generation (NC&CG) algorithm is applied to solve this robust optimization problem. Numerical simulations of two coupled networks are conducted to demonstrate the effectiveness of the proposed robust resilience enhancement scheme**

***Index Terms*—Electric vehicles, fast charging stations, robust resilience enhancement, coupled traffic and power networks, nested column-and-constraint generation algorithm.**

NOMENCLATURE

Abbreviations

EV	Eletric Vehicle
EVA	EVs require charging
EVB	EVs with sufficient electricity
EVC	non-EV
FCS	Fast Charging Station
NC&CG	Nested Column-and-Constraint Generation
PDN	Power Distribution Networks
SOCP	Second-Order Cone Programming
TN	Transportation Networks
V2G	Vehicle-to-Grid

Indices and Sets

$F(b)$	Set of bus
l, b	Index of line and bus
L_e	Set of power line ends
L_s	Set of power line starts
r, a, k	Index of O-D pair, road, and route

Parameters

α, β	Weight coefficients of normal and contingency scenarios
Δch	Conversion factor between charging power of FCS and traffic flow
ΔTC	Conversion factor between traffic flow and charging power
ω	Economic parameter of travel time cost
ϕ	Economic parameter of the load shedding punishment and unserved electric loads
C_a^{rt}	Additional road toll of road a
c_a	Road a capacity
N^B, N^{Sub}	Number of bus and substation
n^{FCS}, n^{V2G}	Real number of charging units and V2G units in each FCS
$N^{line}, N^{FCS}, N^{V2G}$	Maximum number of electric line, fast charging station and V2G devices locations
$P_{max}^{FC}, P_{max}^{V2G}$	Max charging power and supporting power of each charging unit
S_{l0}, S_{b0}^{Sub}	Apparent power capacity of electric line l and bth substation
β_{ka}^r	Incidence coefficient between route traffic flow and road traffic flow

Variables

$\tilde{C}_a^{rt}$	The additional road toll of traveling through each road under contingency state
$\tilde{e}_{k,f}^r$	Binary variable to denote EVAs charging selection of FCS of route k in O-D pair r under contingency state, 1: selected, 0: unselected
$\tilde{e}_{k,v}^s$	Binary variable to denote contingency-supported EVBs supporting selection of FCS of route k in O-D pair s under contingency state, 1-selected, 0-unselected
$\tilde{m}_a, \tilde{t}_a$	Traffic flow and real travel time of road a under contingency state
$\tilde{P}_v^{V2G}$	Supporting power flow of FCS v

This work was supported in part by National Science and Technology Council, Taiwan, R.O.C., under Grant 111-2622-E-007-019, 111-2221-E-007-142, 111-2221-E-019-081, 111-3116-F-018-001, 112-2221-E-007-023, 112 -2927-I-007-505, 112-2123-M-002-010, and 112-2622-E-007-026. *(Corresponding author: Chia-Chi Chu. Co-corresponding author: Wei Gan.)*

Jianfeng Wen is with the Department of Electrical Engineering and Electronics, University of Liverpool, Liverpool, UK, and with the Department of Electrical Engineering, National Tsing Hua University, Hsinchu, Taiwan (e-mail: j.wen7@liverpool.ac.uk; jfwen@m111.nthu.edu.tw).

Wei Gan is with the School of Engineering, Cardiff University, Cardiff, UK (e-mail: ganw4@cardiff.ac.uk).

Chia-Chi Chu is with the Department of Electrical Engineering, National Tsing Hua University, Hsinchu, Taiwan, R.O.C. (email: cc-chu@ee.nthu.edu.tw).

Lin Jiang is with Department of Electrical Engineering and Electronics, University of Liverpool, Liverpool, UK (email: ljiang@liverpool.ac.uk).

Jiajie Luo is with Siemens Gamesa, West Midlands, UK (email: jiajie.luo@siemensgamesa.com).

$\widetilde{CA}^r$ The lowest cost of EVA traveling through O-D pair r under contingency state

$\widetilde{CBC}^r$ The lowest cost of EVB and VC traveling through O-D pair r under contingency state

$\widetilde{CB}^r$ The lowest cost of contingency-supported EVB in O-D pair r under contingency state

$\widetilde{CB}^s$ The lowest cost of EVs in EVB traveling through O-D pair s for grid-supported under the contingency state

$\widetilde{P}_b^{FCS}$ Charging power of FCS at each bus under contingency state

$\widetilde{P}_b^{LS}, \widetilde{Q}_b^{LS}$ Load shedding of active and reactive power at the bth bus under the contingency state

$\widetilde{P}_b^{Sub}, \widetilde{Q}_b^{Sub}$ Active and reactive power of substation at each bus under contingency state

$\widetilde{P}_b^S$ Total power flow of FCS at each bus under contingency state

$\widetilde{P}_l, \widetilde{Q}_l$ Active and reactive loads at each bus under contingency state

$\widetilde{RA}_k^r, \widetilde{RBC}_k^r$ Traffic flow of EVA, contingency-unsupported EVB and VC of route k in O-D pair r under contingency state

$\widetilde{RBC}_{k,v}^s$ Traffic flow which is allocated to FCS with V2G v from EVB in route k, O-D pair r under contingency state

$\widetilde{RB}_k^s$ Traffic flow of contingency-supported EVB of route k in O-D pair r under contingency state

$\widetilde{RB}_v^s$ Supporting traffic flow which is allocated to FCS v

$\widetilde{TB}^s$ Traffic demand of EVs in EVB for grid-supported under the contingency state

$\widetilde{TB}^{se}, \widetilde{TB}^{ss}$ Traffic demand of EVs in EVB for remote and on-site grid-supported under contingency state

C_0^r, C_0^s Ideal travel time cost of vehicles traveling through O-D pair r and s

C_E Cost of purchasing electricity

C_{in}^s Base payment for EVs in EVB traveling through O-D pair s for grid-supported under the contingency state

CA^r The lowest cost of EVA traveling through O-D pair r under normal state

$e_{k,f}^r$ Binary variable to denote EVAs charging selection of FCS of route k in O-D pair r under normal state, 1-selected, 0-unselected

m_a, t_a Traffic flow and real travel time of road a under normal state

P_b^{FCS} Charging power of FCS at each bus under normal state

P_b^L, Q_b^L Active and reactive loads at each bus under normal state

P_b^{Sub}, Q_b^{Sub} Active and reactive power of substation at each bus under normal state

P_f^{FCS} Charging power flow of FCS f

P_l^{Vir} Virtual power flow of line l

R_f^{FCS} Charging traffic flow which is allocated to FCS f

RA_k^r, RBC_k^r Traffic flow of EVA, EVB and VC of route k in O-D pair r under normal state

$RAC_{k,f}^r$ Traffic flow which is allocated to FCS f from EVA in route k under normal state

s Proportion of EVs in EVB that participate in grid-supported

t_a^0 Vehicles travel time in road a without congestion

TA^r, TB^r, TC^r Traffic flow of O-D pair r for vehicles in EVA, EVB and EVC.

z_l, z_l^E, z_l^H Line states, line expanding and line hardening variables

CBC^r The lowest cost of EVB and VC traveling through O-D pair r under normal state

I. Introduction

MORE recently, electrical vehicles (EVs) have been regarded as promising environmentally friendly transportation options due to their energy sustainability and lower emissions. Many countries have already implemented policies to promote EVs and the development of charging infrastructure to achieve the goal of zero-carbon emissions [1]. As a result, a significant number of fast charging stations (FCSs) have been rapidly deployed to meet the growing demand for fast charging. However, the widespread deployment of FCSs can lead to strong interactions between power distribution networks (PDN) and transportation networks (TN) [2]. The transportation mode, travel costs, and charging prices at FCSs can all influence traffic congestion, which, in turn, impacts the location and size of FCSs [3]. In fact, each FCS's high charging power can be considered a significant power load with profound implications for PDNs [4]. Thus, FCS infrastructure establishes inter-dependencies between TN and PDN. These locations of FCSs significantly affect driver behavior, while these capacities of FCSs limit the charging traffic flow within the TN.

Research efforts are being devoted to develop various directions to tackle out this new challenge, including (i) modeling of coupled TN and PDN, (ii) scheduling the location and capacity of FCS, and (iii) TN planning. Initially, several studies addressed the optimal EV charging fees for the customers' side, as documented in [5], and the economic investment plan for coupled TN and PDN, as discussed in [6]–[11]. In particular, [6] introduced a data-based multi-scenario model for coupled traffic and power generation, aiming to jointly optimize both investment and operational costs. [7] utilized deep learning techniques to build a predict-then-optimize diagram to provide traffic flow prediction and build a graph convolutional network for solving the data missing issue. In [8], a mixed-integer convex programming approach was studied for expansion planning of urban electrified transportation networks. In [9], the authors proposed a model for optimal planning of charging stations by a stochastic mixed-integer second-order cone program (SOCP) formulation for optimal planning of charging stations. In [10], a novel reinforcement learning framework within a finite discrete Markov decision process was implemented to deal with the FCS deployment plan. Meanwhile, several comprehensive coupled TN and PDN models have been proposed. For example, in [11], the authors examined the

road capacity expansion scheme under EV driving range. [12] summarized the coupled power-traffic network model across three distinct time scales: long-term, mid-term, and short-term. Several types of models such as time-expanded networks [13] and spatial-temporal model [14] were implemented to minimize the total cost of the coupled network. Consideration of renewable energy was incorporated in the development of coupling network planning schemes that target the utilization of EVs for renewable energy consumption in [15], [16]. [17] delved into the interplay between the market and the coupled system, proposing a market equilibrium strategy to simultaneously benefit the power network and EV drivers. Additionally, [18] concentrated on examining the interaction between vehicles and the electric system along a specific public transport route, with the goal of minimizing the overall operational costs.

Due to severe climate changes in recent years, coupled TN and PDN also face the challenge of maintaining power stability under extreme weather conditions. PDN often suffers significant damage when exposed to natural disasters [19], [20]. In such scenarios, the development of resilient enhancement plans for coupled PDN and TN becomes critical. A common approach to improving resilience is the hardening of the power network. Several hardening solutions, such as over-head structure reinforcement and vegetation management, are commonly employed [21]. For example, [22] proposed a PDN resilience enhancement scheme based on the hardening of power distribution lines. However, this approach may appear impractical due to the high investment required. One alternative solution is to implement flexible resilience enhancement strategies within coupled TN and PDN, leveraging EVs that can be dispatched to different PDN nodes as flexible distributed power sources via the vehicle-to-grid (V2G) mode of EVs [23]. With the rapid growth in the number of EVs, they can play a crucial role as a mobile energy storage system (MESS), which can further enhance the resilience and flexibility of coupled PDN and TN [24]. EVs have been harnessed as flexible resources to support power grid restoration during contingencies [25]. In this direction, [26] proposed a coordinated scheme for determining the site and size of charging stations, with on-site storage to support power grid balance. [27] introduced a distributed model predictive control strategy to regulate PDN voltage and use V2G as a reactive power resource to balance power flow. [28] proposed the virtual electric vehicle energy network to improve the scalability of coupled PDN and TN.

When a natural disaster occurs in the conventional PDN, multiple power distribution lines may suffer from the disaster, the power network cannot recover through the automatic protection. Thus, the demand of electric loads is hardly to be supplied since individual power grid protection schemes may lead to significant losses during the incident [29]. On the other hand, under the framework of coupled PDN and TN, this severe contingency can be easily avoided since EVs may support the PDN as standby MESS via FCSs. Therefore, EVs can be deployed to various PDN nodes as flexible distributed power sources using the V2G mode. Under this situation, the route choice of vehicles, the plan of power distribution lines, locations of FCSs, and uncertainties of traffic flow will result in new challenges to planning and operations of this coupled PDN and TN. The stochastic nature of vehicle operations at each time period poses a challenge. Additionally, unpredictable power distribution line faults during disasters can hinder the design of power network planning and EV dispatching schemes. Therefore, ancillary resilience enhancement with a rational coupled PDN and TN planning become a critical issue.

From our literature survey, it can be concluded that no study has considered the robust resilient planning of coupled PDN and TN in the face of uncertain vehicle flows and contingencies. In this regard, this paper aims to provide a general framework to address this task. The innovations of this work can be summarized as follows:

1) A resilient enhancement scheme by FCSs in coupled PDN and TN is proposed. The planning model incorporates a resilience enhancement strategy that utilizes EV re-dispatching and V2G technologies to support the grid under severe contingencies. In this proposed planning model, both the expansion and hardening of power distribution lines and the placement of FCSs are considered.
2) The planning model is formulated as a two-stage robust optimization problem under uncertainties of EV travel demand. This two-stage model ensures the robustness of the investment scheme and the proposed resilience enhancement strategy, even when faced with varying vehicle travel demands. In the first stage, the model determines the investment plan for power distribution lines and FCSs. In the second stage, it addresses the coupled operation of PDN and TN with uncertainties, involving the optimization of power and traffic flow.
3) To effectively solve the formulated model, a set of linearization techniques is proposed to transform the originally nonlinear problem into a mixed-integer quadratically constrained program. Moreover, by leveraging strong duality theory, the uncertain second-stage operational problem is converted into a deterministic one. Then, a nested column-and-constraint generation (NC&CG) algorithm with dual loops is proposed to solve the first-stage investment problem and the second-stage operational problem iteratively. The outer loop determines the planning scheme, and the inner loop searches for the worst-case travel demand scenarios.

The rest of the paper is organized as follows. Sect. II presents general model descriptions for resilience enhancement of coupled PDN and TN. In Sec. III, model descriptions with uncertainties are considered, and robust optimization techniques are employed to solve this problem. Comprehensive simulation results to validate the effectiveness of the proposed robust resilient enhancement planning scheme are reported in Sec. IV. Finally, some conclusions are made in Sec. V.

II. Resilience Enhancement via EVs

Modeling aspects of the proposed resilience enhancement strategy via EVs will be described in this section. For simplicity, it is assumed that the vehicles in the TN can be categorized into three groups: (a) EVA: EVs that require charging, (b) EVB: EVs with sufficient electricity, and (c) VC: non-EVs.

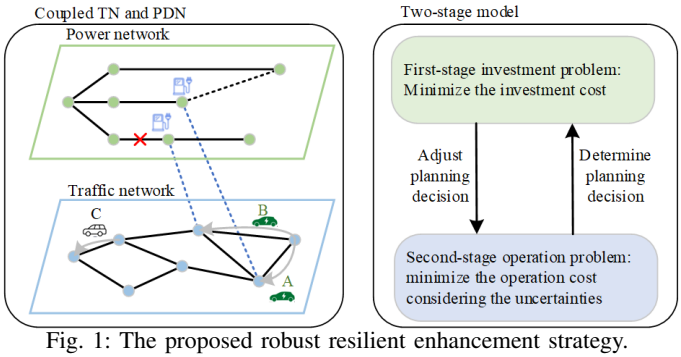

Fig. 1: The proposed robust resilient enhancement strategy.

When power distribution line disconnections occur due to serious natural calamities, certain electric loads may remain unserved despite network reconfigurations. In such situations, EVB is considered as MESS to provide electricity to the PDN through nearby FCSs. Simultaneously, the proposed strategy involves re-dispatching EVA vehicles to be charged at FCSs with adequate electricity supply. Fig. 1 illustrates the concept of the re-dispatching process of EVA and EVB, as well as the proposed two-stage enhanced resilient strategy for charging infrastructure in the coupled PDN and TN under uncertainties.

The coupled model under study consists of three components: (i) the TN model, (ii) the PDN model, and (iii) the FCS model, which serves as the interface that couples the TN and the PDN. Unlike the conventional TN model, various V2G equipment is implemented in the FCS. Therefore, EVBs can support the PDN through FCSs. In situations where power distribution lines suffer severe damage due to extreme weather conditions, these EVBs can serve as a temporary power resource for the PDN. Under such conditions, the power flow of FCSs can be expressed by the following equation:

$$\tilde{P}_b^S = \tilde{P}_b^{FCS} - \tilde{P}_v^{V2G}. \tag{1}$$

It should be noted that these V2G devices are assembled on charging units. Thus, the number of V2G devices should not be more than charging units in each FCS:

$$n^{V2G} \leq n^{FCS}. \tag{2}$$

In addition, we will also consider the uncertain nature of these traffic flows. The varying traffic flows throughout the day and across different seasons have a significant impact on the ability of EVBs to support the grid. To account for this impact, uncertainties stemming from vehicle flows are also included in the second stage of the proposed model.

III. Robust Resilient Enhancement Planning

The proposed EV-based resilient enhancement planning in coupled PDN and TN can be illustrated in Fig. 1. The first stage is the investment problem, while the second stage is the operation problem.

A. Objective

The objective is to minimize the investment and operation cost of both PDN and TN under normal and contingency states. Typically, contingency constructions are considered using an N-1 criterion [30]. Subsequent planning considerations concentrate solely on severe contingencies selected from the N-1 contingency list. Under this framework, the objective can be expressed as:

$$\min\left(I_L + \alpha O_N + \sum_{i=1}^{n} \beta_i O_{Ci}\right), \tag{3}$$

which is composed by three terms I_L, O_N and O_C. I_L represents the investment cost of power distribution lines and charging stations. O_N and O_C are the total operation cost in normal and contingency states respectively. α and β are weight coefficients of normal and contingency scenarios. The determination of weight coefficients relies on empirical evidence as addressed in [36]–[39]. n is the total number of contingency scenarios under study. Their detailed expressions can be described as follows:

$$I_L = c_E z_l^E + c_R z_l^H + c_{FCS}\left(z_n^{FCS} + z_n^{V2G}\right), \tag{4}$$

$$\begin{aligned} O_N = &\sum_r \left[TA^r CA^r + \left(TB^r + TC^r\right) CBC^r\right] \\ &- \sum_r \left(TA^r + TB^r + TC^r\right) C_0^r + C_F \sum_b P_b^{Sub}, \end{aligned} \tag{5}$$

$$\begin{aligned} O_C = &\sum_r \left[TA^r \widetilde{CA}^r + \left((1-s)TB^r + TC^r\right) \widetilde{CBC}^r\right] \\ &- \sum_r \left(TA^r + (1-s)TB^r + TC^r\right) C_0^r \\ &+ \sum_s \widetilde{TB}^{se}\left(\widetilde{CB}^s - C_0^s\right) + \sum_s \widetilde{TB}^s C_{in}^s \\ &+ C_F \sum_h P_h^{Sub} + \varphi\left(\widetilde{P}_h^{LS} + \sum_c \Delta TC \cdot \widetilde{TB}^s \widetilde{CB}^{se}/\omega\right), \end{aligned} \tag{6}$$

where c_E, c_R, and c_{FCS} represent cost coefficients. z_l^E, z_l^H, z_n^{FCS} and z_n^{V2G} are binary variables denoting the planning status of power distribution line expansion, power distribution line hardening, and charging station planning, respectively.

Physical interpretations of each term in (5) and (6) can be illustrated as follows. The first summation term in (5) represents the real travel cost of all types of vehicles, while the second summation term in (5) is the ideal travel cost of all vehicles. In our formulation, each vehicle is assumed to choose the shortest route, avoiding any traffic congestion. Thus, these two terms constitute the actual extra cost of traffic demand, considering traffic congestion with heavy traffic loads. The third summation term in (5) is the electricity network operation cost, containing the total cost of purchasing electricity. On the contrary, the first two summation terms in (6) are similar to those in (5). However, a variable 's' is appended to EVB-type EVs. Therefore, the travel cost of EVBs that participate in grid support is excluded and placed in the third term alone. A fundamental fee is paid to the grid-supported EVs to stimulate their participation, and this is included in the fourth summation term of (6). The fifth summation term in (6) represents the electricity network operation cost under congestion states. Finally, the last summation term in (6) relates to those electric loads that remain unserved, including some loads under load shedding actions and those loads that were already unserved before the grid-supported EVs arrived at the destination charging station.

B. First Stage Constraints

In the first stage, planning schemes are developed for both power distribution lines and FCSs. The FCS planning scheme encompasses not only the sitting of FCSs but also the selection of FCSs equipped with V2G technology. (7) and (8) ensure that the total numbers of expanded lines, hardened lines, and charging stations fall within reasonable ranges.

$$\sum_{l} z_l^E \le N^{\text{line}}, \ \sum_{l} z_l^H \le N^{\text{line}}, \tag{7}$$

$$\sum_{n} z_n^{FCS} \le N^{FCS}, \ \sum_{n} z_n^{V2G} \le N^{FCS}, \tag{8}$$

where z_l^E, z_l^H, z_n^{FCS}, and z_n^{V2G} are binary variables to be determined if these devices or planning are implemented.

After planning the power distribution line, its capacity c_l can be represented by (9). The planning scheme also affects the connection state of electric lines. If a electric line is hardened, this line remains connecting regardless of the disaster. These V2G devices should be implemented to pre-existing FCSs. Thus, EVs can only support the power grid through FCSs with V2G devices.

$$S_l = z_l^E S_{l0}. \tag{9}$$

C. Second Stage Constraints Under Normal State

Different from the planning scheme studied in the first stage, the model of coupled PDN and TN under the normal state and the contingency state are different in the second stage. Detailed descriptions will be stated below.

1) PDN Constraints under Normal States: In the second stage, both power flow in the PDN and traffic flow in the TN are addressed. A simplified lossless AC power flow in a radial PDN is adopted [8]. The initial line status variable z_l describes the network topology. The equivalent formulation is described by (10) and (11). This set of constraints ensures the connectivity of each bus in the radial PDN.

$$\sum_{l} z_l \le N^B - N^{Sub}, \ -M_l \cdot z_l \le P_l^{Vir} \le M_l \cdot z_l, \tag{10}$$

$$\sum_{l \in L_s} P_l^{Vir} - \sum_{l \in l_e} P_l^{\text{Vir}} = -1. \tag{11}$$

The active power and reactive power balance equation will be denoted by (12) and (13) respectively. The power flow of FCSs is also included in (12).

$$P_b^{Sub} - P_b^L - P_b^{FCS} = \sum_{l \in L_s} P_l - \sum_{l \in L_e} P_l, \tag{12}$$

$$Q_b^{Sub} - Q_b^L = \sum_{l \in L_s} Q_l - \sum_{l \in L_e} Q_l. \tag{13}$$

(14) expresses the voltage drop of each line and the line voltage lies in the tolerance range:

$$U_{L_s} - U_{L_e} = r_l P_l + x_l Q_l, \ U_b^{\min} \le U_b \le U_b^{\max}. \tag{14}$$

Substation and line constraints are described by (15).

$$S_b^{Sub} \ge \sqrt{\left(P_b^{Sub}\right)^2 + \left(Q_b^{\text{Sub}}\right)^2}, \ \ S_l \ge \sqrt{(\text{P}_l)^2 + (Q_l)^2}. \tag{15}$$

2) TN Constraints Under Normal States: In the TN, constraints primarily describe the relationship between traffic flow on roads, paths, and traffic demands. In this context, we use Origin-Destination (O-D) pairs to describe the origin and destination of each vehicle. Each O-D pair may contain several routes, and each route is composed of several roads. Traffic demand balance constraints are presented in (16):

$$\sum_{k} RA_k^r = TA^r, \ \sum_{k} RBC_k^r = TB^r + TC^r. \tag{16}$$

The traffic demand of the routes set in each O-D pair is related to the roads. The traffic flow balance for EVs in each category is given by (8). (17) describes the relationship between road traffic flow and route traffic flow of EVs through the incidence coefficient β_{ka}^r.

$$m_a = \sum_{r} \sum_{k} \left(RA_k^r + RBC_k^r\right) \beta_{ka}^r. \tag{17}$$

A typical Bureau of Public Roads function which demonstrates the relationship between real travel time t_a and road traffic flow is stated in (18):

$$t_a = t_a^0 \left[1 + 0.15 \left(m_a / c_a\right)^4\right]. \tag{18}$$

(19) depicts the real travel cost for vehicles using route k within the O-D pair r, in which the additional road toll for each road is also considered.

$$C_k^r = \sum_{a} \left(\omega t_a + C_a^{rt}\right) \beta_{ka}^r. \tag{19}$$

Here we adopt the user equilibrium principle, ensuring that in each O-D pair, all vehicles must select the route with the lowest travel cost.

$$RA_k^r \cdot (C_k^r - CA^r) = 0, \ RA_k^r \ge 0, (C_k^r - CA^r) \ge 0, \tag{20}$$

$$RBC_k^r \cdot (C_k^r - CBC^r) = 0, \ RBC_k^r \ge 0, (C_k^r - CBC^r) \ge 0. \tag{21}$$

3) FCSs Constraints Under Normal States: Since FCSs serve as coupling facilities between the PDN and the TN, FCS constraints primarily describe the relationship between traffic flow and charging demands or discharging power provided by grid-support EVs. In this work, (22) relates the traffic flow of EVA on route k and each FCS through $e_{k,f}^r$, and the total traffic flow of EVA allocated to each FCS.

$$RAC_{k,f}^r = e_{k,f}^r RA_k^r, \ R_f^{FCS} = \sum_{r,k} RAC_{k,f}^r. \tag{22}$$

Despite the charging traffic flow balance of each route, the charging demand of each O-D pair also needs to be satisfied as follows:

$$\sum_{k,f} RAC_{k,f}^r = TA^r. \tag{23}$$

(24) establishes the relationship between the charging traffic flow of each FCS and the corresponding charging power flow at that FCS. This captures the coupling effect of the TN on the PDN and the total charging power should be within an available range. The maximum charging power of each FCS depends on the total number of charging units invested at each FCS. The charging power flow of each bus is determined by (25), which aggregates all the charging power from FCSs connected to the bus.

$$R_f^{FCS} \Delta ch = P_f^{FCS}, \ \ 0 \le P_f^{FCS} \le P_{\max}^{FCS} \cdot N^{FCS}, \tag{24}$$

$$P_b^{FCS} = \sum_{f \in F(b)} P_f^{FCS}. \tag{25}$$

D. Second Stage Constraints Under Contingency States

Since faults in the PDN are considered in the contingency state, and EVs will participate in PDN support via FCSs equipped with V2G for the re-dispatch scheme, the charging

and supporting power flow will change, and the power flow within the PDN will be redistributed. Under this strategy, EVBs will change their destinations and move to assigned charging stations to support the PDN. Therefore, the traffic flow of all vehicles will be re-allocated by the TN.

1) PDN Constraints Under Contingency States: When a contingency occurs under abnormal conditions, the connectivity status of each power distribution line will also change. Thus, the connection status of each line can be described by:

$$\tilde{z}_l = 0,\ \forall l \in l_d. \tag{26}$$

(27) depicts the connection status of each line. When a line is planned to be hardened, it maintains its connection status even if the line is attacked under contingency conditions.

$$c_l \geq z_l^H, c_l \geq \tilde{z}_l. \tag{27}$$

The active and reactive power flow balance under the contingency state is described by constraints (28) and (29).

$$\tilde{P}_b^{Sub} - P_b^L - \tilde{P}_b^{FCS} + \tilde{P}_b^{LS} = \sum_{l\in L_s} \tilde{P}_l - \sum_{l\in L_e} \tilde{P}_l, \tag{28}$$

$$\tilde{Q}_b^{\text{Sub}} - Q_b^L + \tilde{Q}_b^{LS} = \sum_{l\in L_s} \tilde{Q}_l - \sum_{l\in L_e} \tilde{Q}_l. \tag{29}$$

Compared to these constraints under normal conditions as shown in Sec. III.C, load shedding actions are considered in (28) and (29) due to the insufficient power line capacity under fault conditions. Constraints (12) to (14) under normal states must also be satisfied.

2) TN Constraints Under Contingency States: If the power line capacity cannot meet the load demand under the contingency state, load shedding may occur to balance the power supply. In such a situation, EVBs that have sufficient electricity will provide power support to the PDN via FCSs equipped with V2G technology. This model provides an EVB re-dispatching strategy aimed at minimizing the total cost of the coupled network. (30) describes the portion of EVs participating in power support in EVBs.

$$\sum_r sTB^r = \sum_s \widetilde{TB}^s. \tag{30}$$

This category of EVs contains two terms, as shown in (31):

$$\sum_s \widetilde{TB}^s = \sum_s \left(\widetilde{TB}^{se} + \widetilde{TB}^{ss}\right). \tag{31}$$

EVs will go to nearby FCSs to provide V2G support onsite. The traffic demand balance under the contingency state is shown in (32) and (33):

$$\sum_k \widetilde{RB}_k^s = \widetilde{TB}^s,\ \sum_k \widetilde{RA}_k^r = TA^r, \tag{32}$$

$$\sum_k \widetilde{RBC}_k^r = (1-\mathrm{s})TB^r + TC^r. \tag{33}$$

The relationship between road traffic flow and route traffic flow is described by:

$$\widetilde{m}_a = \sum_r \sum_k \left(\widetilde{RA}_k^r + \widetilde{RBC}_k^r\right)\beta_{ka}^r + \sum_s \sum_k \widetilde{RB}_k^s \beta_{ka}^r. \tag{34}$$

From (34), the travel time of each road is depicted by

$$\tilde{t}_a = t_a^0\left[1 + 0.15\left(\widetilde{m}_a/c_a\right)^4\right]. \tag{35}$$

(36) describes the travel cost of EVA under the contingency state, considering additional charging fees and road tolls:

$$\widetilde{CA}_k^r = \sum_r \tilde{C}_r^{FCS}\tilde{e}_{k,f}^r + \sum_a \left(\omega\tilde{t}_a + \tilde{C}_a^{rt}\right)\beta_{ka}^r. \tag{36}$$

(37) ensures that each car needing charging selects only one FCS:

$$\sum_n \tilde{e}_{k,f}^r \leq 1. \tag{37}$$

Compared to (36), the travel cost of contingency-unsupported EVBs and VCs does not include charging fees, and road tolls are omitted from the travel cost of contingency-supported EVBs in (38).

$$\widetilde{CBC}_k^r = \sum_a \left(\omega\tilde{t}_a + \tilde{C}_a^{rt}\right)\beta_{ka}^r,\ \widetilde{CB}_k^s = \sum_a \omega\tilde{t}_a\beta_{ka}^r. \tag{38}$$

(39), (40), and (41) ensure that the user equilibrium is satisfied in the contingency state.

$$\widetilde{RA}_k^r \cdot \left(\widetilde{CA}_k^r - \widetilde{CA}^r\right) = 0, \tag{39}$$

$$\widetilde{RBC}_k^r \cdot \left(\widetilde{CBC}_k^r - \widetilde{CBC}^r\right) = 0, \tag{40}$$

$$\widetilde{RB}_k^s \cdot \left(\widetilde{CB}_k^r - \widetilde{CB}^s\right) = 0. \tag{41}$$

3) FCS Constraints Under Contingency State: In the contingency state, the charging requirements of EVAs are fulfilled priority. The contingency-supported EVBs will support the PDN via FCS equipped with V2G technology. The contingency-supported traffic flow allocated to each FCS implemented with V2G devices is determined by (42).

$$\widetilde{RBC}_{k,v}^s = \tilde{e}_{k,v}^s\widetilde{RB}_v^s,\ \tilde{R}_v^{V2G} = \sum_{s,k}\widetilde{RBC}_{k,v}^s,\ \sum_{k,v}\widetilde{RBC}_{k,v}^s = \widetilde{TB}^s. \tag{42}$$

(43) specifies the grid-supporting power derived from the contingency-supported EVBs' traffic flow, and restricts the total supporting power within the allowed range. (44) depicts the charging power flow of each bus under contingency.

$$\tilde{R}_v^{V2G}\Delta ch = \tilde{P}_v^{V2G},\ 0 \leq \tilde{P}_f^{V2G} \leq P_{\max}^{V2G}\cdot N^{V2G}, \tag{43}$$

$$\tilde{P}_b^{FCS} = \sum_{f\in F(b)} \tilde{P}_f^{FCS} - \sum_{v\in F(b)} \tilde{P}_v^{V2G}. \tag{44}$$

IV. Robust Planning Under Uncertainty

A. Descriptions of the Uncertainty Set

To address these uncertainties in traffic flow, the variable representing traffic flow at time t, denoted as $M_{n,t}$, is treated as falling within an interval of $[-\Delta M_{n,t}, \Delta M_{n,t}]$ around its forecasted value, which is denoted as $M_{n,t}^0$. This interval represents the range of potential deviations from the forecasted value. An uncertainty budget, denoted as Γ, where $0 \leq \Gamma \leq T$, is introduced to modify the robust planning conservatism coefficient. The uncertainty set is defined by (45), which presumably outlines the specific mathematical representation of the uncertainty set.

$$\chi = \left\{ M_{n,t} \in R^{N_n\times T},\ \sum_{t=1}^{T}\left(y_t^{S+} + y_t^{S-}\right) \leq \Gamma_n, \right.$$
$$\left. M_{n,t} = M_{n,t}^0 + \left(y_t^{S+} - y_t^{S-}\right)\Delta M_{n,t} \right\}. \tag{45}$$

After incorporating these uncertainty terms, the robust planning model aims to find the optimal solution within the range of upper and lower bounds of uncertainty scenarios. This means that the model will take into account the uncertainty in traffic flow represented by $\Delta M_{n,t}$ and the uncertainty budget Γ when making planning decisions, ensuring that the plan remains robust and adaptable to potential variations in traffic conditions.

B. Linearization

It is noteworthy that $\widetilde{TB}^s \widetilde{CB}^{se}$ in (6) is a nonlinear function which is composed by multiplications of two continuous decision variables. To simplify its computation, the linearization technique will be exploited. First, $\widetilde{TB}^s$ is chosen to be discretized and expressed by a binary variable w_j^s as shown below:

$$\widetilde{TB}^s = \Delta TB \sum_{j=1}^{J} 2^{j-1} w_j^s. \tag{46}$$

With w_j^s, $\widetilde{TB}^s$ can be divided into several intervals and the length of each interval is ΔTB. The value of $\widetilde{TB}^s$ depends on the chosen of j. Now $\widetilde{TB}^s \widetilde{CB}^{se}$ can be re-written as (47) by using (46) to represent $\widetilde{TB}^s$. Thus, this item is converted into a continuous variable multiplying a binary variable as follows:

$$\widetilde{TB}^s \cdot \widetilde{CB}^{se} = \Delta TB \sum_{j=1}^{J} 2^{j-1} w_j^s \widetilde{CB}^{se}. \tag{47}$$

After such a replacement, the big-M method can be applied to (47) and $\widetilde{TB}^s \widetilde{CB}^{se}$ will be replaced by (47), (48), and (49).

$$-bigM \cdot \left(1 - w_j^s\right) \le w_j^s \widetilde{CB}^{se} - \widetilde{CB}^{se} \le bigM \cdot \left(1 - w_j^s\right), \tag{48}$$

$$-bigM \cdot w_j^s \le w_j^s \widetilde{CB}^{se} \le bigM \cdot w_j^s. \tag{49}$$

M is a large number containing all possible values of $\widetilde{CB}^{se}$.

It is worthy of noting that the linearization of (20) and (21) can be accomplished using the big-M method. The procedure aligns with the approach applied to handle (47)-(49). To maintain conciseness, we omit technical details.

C. Robust Optimization

After considering the uncertainty set, the original optimization problem will be converted into the following two-stage robust problem (50):

$$\begin{aligned} &\min_{\boldsymbol{C},\boldsymbol{Z}} \boldsymbol{\mu}^T \cdot \boldsymbol{C} + \max_{\boldsymbol{M}\in\boldsymbol{\chi}} \min_{\boldsymbol{D},\boldsymbol{U}} \boldsymbol{\sigma}^T \cdot \boldsymbol{D} \\ &\text{s.t. } \boldsymbol{\phi C} + \boldsymbol{\varphi Z} \le \boldsymbol{h}, \boldsymbol{\kappa C} + \boldsymbol{\lambda Z} + \boldsymbol{\theta U} + \boldsymbol{\vartheta D} \le \boldsymbol{\gamma(M)}, \\ &\quad \boldsymbol{Z} \in \{0,1\},\ \boldsymbol{U} \in \{0,1\}. \end{aligned} \tag{50}$$

where $\boldsymbol{\phi C} + \boldsymbol{\varphi Z} \le \boldsymbol{h}$ is the first stage constraint. $\boldsymbol{C}$ and $\boldsymbol{Z}$ are the continuous and binary variables. $\boldsymbol{\kappa C} + \boldsymbol{\lambda Z} + \boldsymbol{\theta U} + \boldsymbol{\vartheta D} \le \boldsymbol{\gamma(M)}$ is the second stage constraint. $\boldsymbol{D}$ and $\boldsymbol{U}$ are the continuous and binary variables. $\boldsymbol{\gamma(M)}$ represents the traffic flow uncertain variable and its a linear function with respect to uncertain variable $M_{n,t}$. $\boldsymbol{\mu}$, $\boldsymbol{\sigma}$ and $\boldsymbol{h}$ are these coefficient vectors in two stages. $\boldsymbol{\kappa}$, $\boldsymbol{\lambda}$, $\boldsymbol{\theta}$, $\boldsymbol{\vartheta}$, $\boldsymbol{\phi}$ and $\boldsymbol{\varphi}$ are coefficient matrices. Detailed developments are shown in Appendix A.

Benders decomposition and the column-and-constraint generation (C&CG) algorithm are both widely used techniques for addressing the two-stage optimization problem [33]–[35]. However, in our specific problem formulation, the second-stage problem remains non-convex due to the presence of binary variables. As a result, the strong duality theory is not applicable for dualizing the second-stage problem. Consequently, we will employ the nested C&CG (NC&CG) algorithm in this study to tackle this problem.

The NC&CG algorithm involves breaking down the optimization problem into two nested loops [35]. In the outer loop, we focus on the master problem concerning planning variables. This is achieved by solving the first-stage problem utilizing scenarios acquired from the inner loop. The inner loop is designed to identify the worst-case scenarios by solving the second-stage problem. In this optimization problem, the outer loop encompasses the planning of the electricity grid, the determination of FCS locations, and the placement of V2G devices. The operational solution will be derived from the inner loop solver.

1) Outer loop: In the outer loop, the master problem is resolved to ascertain the planning variables for the integrated network, taking into account the most adverse scenario identified in the inner loop's sub-problem. The following procedure shows the algorithm for solving the master problem in the outer loop:

1) Set the lower bound (LB) of the master problem as $-\infty$, set the upper bound (UB) of the problem as $+\infty$, and $m = 0$;
2) Solve the master problem (51) to derive an optimal solution C^* and update the lower bound $LB^{out} = \varepsilon$:

$$\begin{aligned} &\min_{\boldsymbol{C},\boldsymbol{Z}} \boldsymbol{\mu}^T \cdot \boldsymbol{C} + \varepsilon \\ &\text{s.t. } \boldsymbol{\phi C} + \boldsymbol{\varphi Z} \le \boldsymbol{h}, \\ &\quad \varepsilon \ge 0,\ \boldsymbol{Z} \in \{0,1\}. \end{aligned} \tag{51}$$

3) Solve the sub-problem in the inner loop with the optimal solution obtained by the outer loop to update the upper bound UB^{out} of the master problem.
4) If $|UB^{\text{out}} - LB^{\text{out}}| \le \epsilon$, return the planning variables and terminate the outer loop. Otherwise set $m = m + 1$, do the following constraint (52) and go back to step 2).

$$\begin{aligned} \boldsymbol{\kappa C} + \lambda \boldsymbol{Z} + \boldsymbol{\theta U^m} + \boldsymbol{\vartheta D^m} \le \boldsymbol{\chi^*} \\ \boldsymbol{U^m} \in \{0,1\}. \end{aligned} \tag{52}$$

2) Inner loop: The inner loop focuses on solving the sub-problem to seek the worst scenario with respect to the objective function of the master problem [40]–[42]. The algorithm can be outlined as follows:

1) Preset $\boldsymbol{U}$ as an initial value $\boldsymbol{U^{n*}}$, set the lower bound of the sub-problem $LB^{in} = -\infty$, the upper bound of the sub-problem $UB^{in} = +\infty$, and $n = 1$.
2) Solve the sub-problem 1 (53) to update the upper bound $UB^{in} = \tau^*$, and seek the worst scenario $\boldsymbol{\chi^*}$:

$$\begin{aligned} &\max_{\boldsymbol{M}\in\chi} \tau \\ &\text{s.t. } \tau \le (\boldsymbol{\gamma} - \boldsymbol{\phi C}^* - \lambda \boldsymbol{Z}^* - \boldsymbol{\theta U}^{n*})^{\boldsymbol{T}} \boldsymbol{\gamma(M)}^n, \\ &\quad \boldsymbol{\vartheta^T} \lambda^n = \boldsymbol{\sigma}^T,\ \tau > 0. \end{aligned} \tag{53}$$

3) Solve the sub-problem 2 (54) to update the lower bound

$LB^{in} = \max\left\{\boldsymbol{\sigma}^T \cdot \boldsymbol{D}, LB^{in}\right\}$, and obtain the inner loop optimal solution $\boldsymbol{D}$:

$$\begin{aligned} &\min_{\boldsymbol{D},\boldsymbol{U}} \boldsymbol{\sigma}^T \cdot \boldsymbol{D} \\ &\text{s.t. } \boldsymbol{\kappa C}^* + \boldsymbol{\lambda Z}^* + \boldsymbol{\theta U} + \boldsymbol{\vartheta D} \le \boldsymbol{\chi}^*, \\ &\boldsymbol{U} \in \{0,1\}. \end{aligned} \tag{54}$$

4) If $\left|UB^{\text{in}} - LB^{\text{in}}\right| \le \epsilon$, return the UB^{in} and set $UB^{out} = UB^{in}$ to represent the worst scenario $\boldsymbol{\chi}^*$ for the master problem and terminate the outer loop. Otherwise set $n = n+1$, add the following constraint (55) and go back to step 2):

$$\begin{aligned} &\tau \le \left(\boldsymbol{\gamma} - \boldsymbol{\phi C}^* - \lambda \boldsymbol{Z}^* - \boldsymbol{\theta U}^{n*}\right)^{\boldsymbol{T}} \gamma^n, \\ &\boldsymbol{\vartheta}^{\boldsymbol{T}} \lambda^n = \boldsymbol{\sigma}^{\boldsymbol{T}}. \end{aligned} \tag{55}$$

D. Solution Algorithm

In summary, the algorithm of applying the NC&CG algorithm to solve the robust resilient enhancement planning of charging infrastructure in coupled PDN and TN under uncertainties can be stated as follows:

1) Initialize the coupled model;
2) Set the master problem $LB^{out} = -\infty$, $UB^{out} = +\infty$, and $m = 0$;
3) Solve the master problem (51) to obtain solution $\boldsymbol{C}^*$ and the updated LB^{out};
4) set the sub-problem $LB^{in} = -\infty$, $UB^{in} = +\infty$, and $n = 1$;
5) Solve the sub-problem 1 (53) to determine the worst scenario and update the upper bound UB^{in};
6) Solve the sub-problem 2 (54) to update LB^{in};
7) If $\left|UB^{\text{in}} - LB^{\text{in}}\right| \le \epsilon$, set $UB^{out} = UB^{in}$, otherwise set $n = n+1$, update $\boldsymbol{Z}^*$ and go back to step 5);
8) If $|UB^{\text{out}} - LB^{\text{out}}| \le \epsilon$, return the scheduling variables and terminate the outer loop. Otherwise set $m = m+1$, update $\boldsymbol{\chi}^*$ and add constraint (55), then go back to step 3).

In order to illustrate the procedural steps of the NC&CG algorithm, its flowchart is presented in Fig. 2.

E. Computational Complexity

Generally, the NC&CG algorithm is expected to deliver superior performance when compared to the conventional Bender-dual algorithm [35]. Specifically, if p is the number of extreme points of χ, and q is the number of extreme points of γ, then the Benders-dual algorithm and NC&CG algorithm are anticipated to generate an optimal solution in $O(pq)$ and $O(q)$ iterations, respectively. As indicated in [35], even the NC&CG algorithm solves the master program with a larger number of variables and constraints in comparison with the Benders-dual algorithm, under the relatively complete recourse assumption, the number of iterations in the NC&CG algorithm can be reduced by the order of $O(q)$ if the second-stage decision problem is a linear programming. Therefore, as the coupled TN and PDN model in this study is linearized, the scalability of the proposed model is expected to increase linearly. The computational study in the next section will confirm this issue.

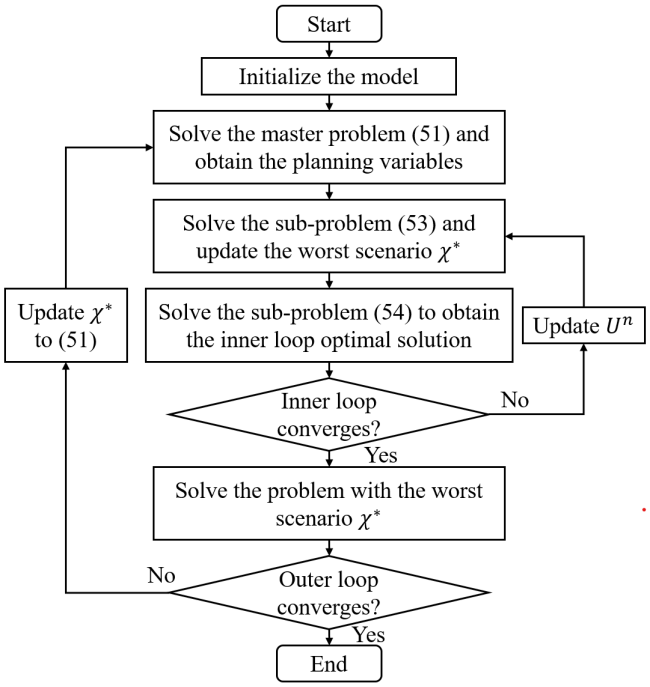

Fig. 2: The flowchart of the NC&CG algorithm.

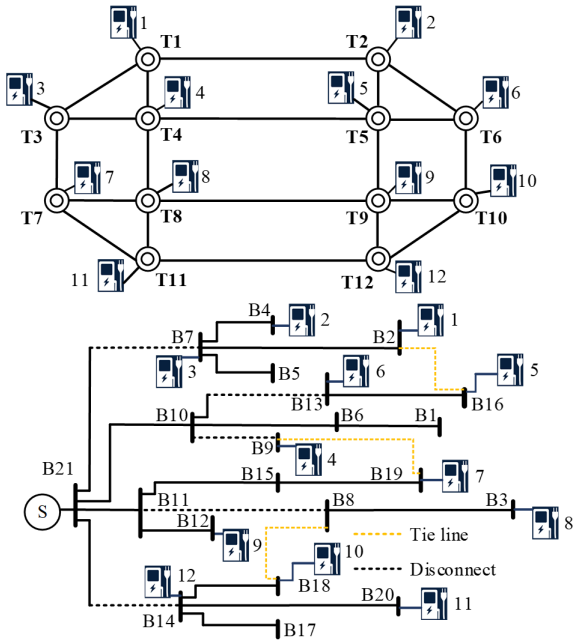

Fig. 3: Structure of test coupled TN and PDN network.

V. Simulation Studies

To demonstrate the effectiveness of the proposed robust resilience enhancement scheme, numerical studies on two coupled TN and PDN are investigated. The first one is the coupled 12-node TN and 21-bus PDN, while the second one is the coupled 24-node TN and 42-bus PDN. A comprehensive analysis is presented below.

A. Coupled 12-Node TN and 21-Bus PDN

First, a coupled 12-node TN and 21-bus PDN, as shown in Fig. 3, will be investigated. Under contingency state, several power distribution lines are destroyed by the natural

disaster and disconnect. The electricity purchase cost is 141 $/MWh, and the travel time cost of vehicles is set as 0.33 $/min. Detailed system information can be found in [31]. Various scenarios are designed to verify the effectiveness of V2G supporting and the enhanced resilience V2G supporting strategy. Simulations are performed on Matlab 2022b platform with embedded Gurobi.

1) Resilient Enhancement Planning Without Uncertainty: First, the resilient enhancement planning without uncertain traffic flow is investigated. Three cases are designed to validate the effectiveness of the proposed V2G supporting strategy under the contingency state:

- Case 1: TN and PDN are planned separately.
- Case 2: The plan is made for the coupled TN and PDN under contingency without EVs support.
- Case 3: The plan is made for the coupled TN and PDN under contingency. Moreover, EVBs will participate in the PDN supporting.

Note that since the uncertainty of traffic loads is not considered in scenario studies in these three cases, the un-served loads are required to be minimized. Table I shows these planning results and Table II depicts their investment cost. Their comprehensive examinations are presented as follows.

- Case 1: Three power distribution lines are selected for reinforcement, with two of them classified as main lines. In this scenario, only one of the main lines is extended, ensuring that, in the event of a contingency, this line can adequately supply power. However, when more main lines are incorporated into the plan, the cost of electric line planning in Case 1 becomes the highest.
  FCSs are positioned at six available sites, but their locations within the PDN are widely scattered. In this instance, the impact on the PDN is not factored in during the FCS design process. As a result, a maximum charging power limit must be imposed to ensure that the lines' capacity can meet the charging power requirements. The dispersed placement of FCSs necessitates the hardening and expansion of main electric lines. Although this planning approach helps avert load shedding, it results in a considerable overall cost for the integrated network, particularly in terms of electric line planning expenses.
- Case 2: We have a plan to reinforce two power distribution lines, with just one of them serving as the primary line. Line B21-B14 is disconnected, leading to unmet power demand for loads connected to this line and rendering the FCS located on this line inoperative. Instead, EVAs traveling on these routes will opt to charge at FCSs connected to B21-B7 and B11-B12 lines, necessitating an expansion of capacity for these two lines. The placement of charging stations also leans more toward these lines. The planning scheme of this case is shown in Fig. 4. In comparison to Case 1, the cost of electric line planning decreases. However, there is a significant increase in load shedding under contingency. Since the likelihood of natural disasters is relatively low, the impact of load shedding on the overall cost is limited.
- Case 3: Two lines are hardened, with only one of them slated for expansion, which is demonstrated in Fig. 5. In the figure, the FCS with V2G is marked as red asterisk. Importantly, no additional primary lines are selected for planning following the integration of V2G-enabled EVs into the grid. This strategy leads to a significant 17% reduction in the total cost of the integrated network while simultaneously curbing load shedding and maintaining it within an acceptable range when compared to Case 2. In this configuration, six FCSs are strategically positioned, which is more than in Case 2. This increase is due to the incorporation of V2G modules. Additionally, three V2G modules are installed in three FCSs, enhancing the power support derived from EVBs.

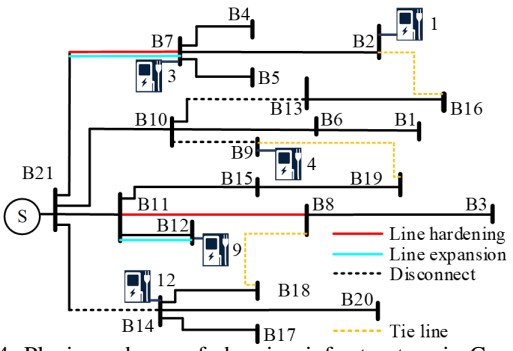

Fig. 4: Planing scheme of charging infrastructure in Case 2.

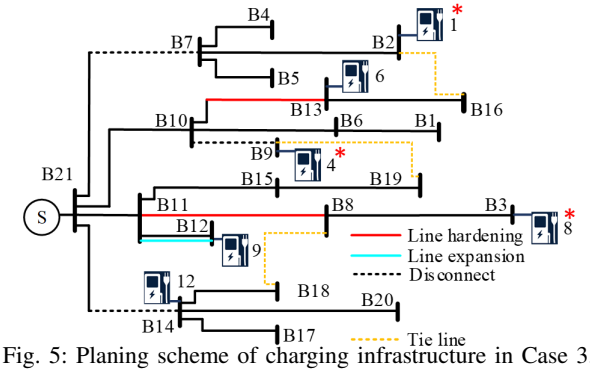

Fig. 5: Planing scheme of charging infrastructure in Case 3.

2) Robust Resilient Enhancement Planning: Now the robust resilient enhancement planning is investigated. The uncertainty of traffic flow is considered in the coupled network plan. Two additional cases under contingency state are designed:

- Case 4: The planning of the coupled network is conducted in a contingency state, where the total traffic flow is predictable and kept constant. However, the proportion of EVBs among all EVs is uncertain.
- Case 5: The coupled network planning under the contingency state takes into account uncertainties in the traffic flow for each type of vehicle. Additionally, there is uncertainty assumed in the total traffic flow.

The fluctuation of the traffic flow is set to be $\pm 15\%$. Table III shows the planning cost and the total cost in each case. From Table III, the following observations can be made:

1) In Case 4, the power line planning cost is more than double those of Case 3, resulting in a 12% increase in total cost compared to Case 1. This fact addresses the

TABLE I: RESILIENT ENHANCEMENT WITHOUT UNCERTAINTY FOR THE COUPLED 12-NODE TN AND 21-BUS PDN

Case	Action	Results	Load Shedding (MWh)
1	Line Hardening	B21-B7, B21-B14, B10-B13	0
	Line Expansion	B21-B14	
	FCS Location	T1, T4, T5, T7, T8, T12	
2	Line Hardening	B21-B7, B11-B8	1.4362
	Line Expansion	B21-B7, B11-B12	
	FCS Location	T1, T3, T4, T9, T12	
3	Line Hardening	B10-B13, B11-B8	0.5871
	Line Expansion	B11-B12	
	FCS Location	T1, T4, T6, T8, T9, T12	
	V2G Location	T1, T4, T8	

TABLE II: COST ($) COMPARISON OF RESILIENT ENHANCEMENT SCHEMES FOR THE COUPLED 12-NODE TN AND 21-BUS PDN

Action	Case 1	Case 2	Case 3
Line Hardening & Expansion	18867	14220	5698
FCS Planning	7776	6480	7776
V2G Implementation	0	0	1166
Operation under Normal State	14989	14968	14989
Operation under Contingency	1727	2485	1498
Extra Contingency-Supported EVBs	0	0	553
Total	43359	38153	31680

TABLE III: COST ($) COMPARISON OF ROBUST RESILIENT ENHANCEMENT SCHEMES FOR THE COUPLED 12-NODE TN AND 21-BUS PDN

Action	Case 3	Case 4	Case 5
Line Hardening & Expansion	5698	9097	8833
FCS Planning	7776	9072	9072
V2G Implementation	1166	778	1166
Total	31680	37147	39390

significant influence of the proportion of EVBs on the planning of the coupled PDN and TN.

2) When comparing Case 3 to Case 5, both the line planning costs and the FCS planning costs are notably higher in Case 5. As a result, it becomes essential to devise distinct strategies for electric lines, FCSs, and V2G modules to address the uncertainties in traffic flow. The total cost of Case 5 exceeds that of Case 3 by 24%, indicating that the coupled network's planning approach in certain conditions struggles to effectively manage traffic flow uncertainties.
3) The number of scenarios considered in Case 5 is considerably larger than in Case 4. Consequently, the total cost of Case 5 is 6% higher than that of Case 4. Thus, more V2G modules are incorporated in Case 5.

In Fig. 6, results across various traffic demand fluctuation rates are provided. The total cost of the integrated network climbs from $31,680 to $42,205. With the increasing fluctuation rate, there is a corresponding rise in the total cost. Notably, the cost increases by $1,443 as the fluctuation rate progresses from 0% to 5%. Similarly, there is an approximate increment of 3000$ in each subsequent range: 5%-10%, 10%-15%, and 15%-20%. This trend indicates that as traffic fluctuations become more pronounced, greater investment is necessary for the planning and operation of the integrated network.

B. Coupled 24-Node TN and 42-Bus PDN

To assess the scalability of the proposed co-planning method, an expanded coupled 24-node TN and 42-bus PDN

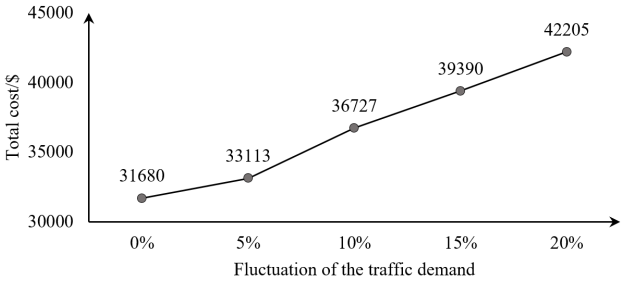

Fig. 6: Total cost under different fluctuation rate of the traffic demand.

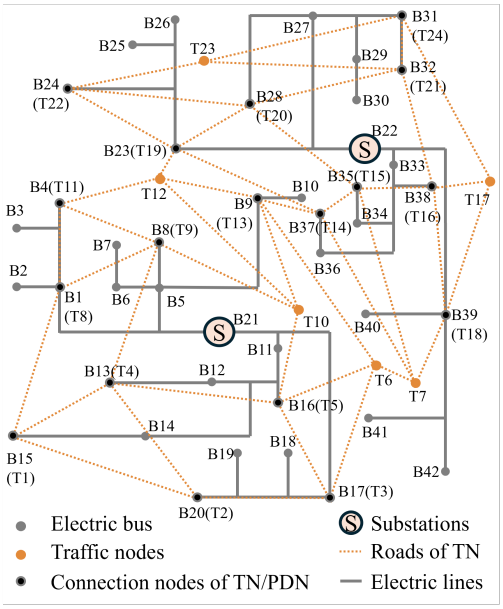

Fig. 7: Structure of coupled 24-Node TN and 42-Bus PDN.

is employed in Fig. 7. This investigation also includes an analysis of the flexibility of V2G EVs. Notably, the impact of natural disasters on the TN is taken into account in this study, with a decrease in the rated capacity of roads affected by disasters. The detailed model of the new road capacity for the contingency state is provided in Appendix B.

1) Case Studies: The expanded model, implemented using the proposed method, has been evaluated in three cases:

- Case 6: The planning of the expanded coupled TN and PDN is conducted without V2G implementation and considers uncertainty under the contingency state.
- Case 7: The planning involves the expanded coupled TN and PDN with EVs support under the contingency state but does not take uncertainty into account.
- Case 8: The planning includes the expanded coupled TN and PDN with consideration for V2G support and uncertainty under the contingency state.

In Case 8, the traffic flow fluctuation is set to be $\pm 15\%$, and the total cost, as well as the cost of each item, are presented in Table IV.

2) Adaptability of the Proposed Planning Method: The economic results demonstrate the adaptability of our proposed planning method. A comparison between the outcomes of Case 6 and Case 7 reveals that V2G implementation significantly reduces the total cost and load shedding when the coupled network is damaged. In Case 8, the cost of FCS and V2G

TABLE IV: COST ($) COMPARISON OF ROBUST RESILIENT ENHANCEMENT SCHEMES FOR THE COUPLED 24-NODE TN AND 42-BUS PDN

Action	Case 6	Case 7	Case 8
Line Hardening & Expansion	18042	6477	19646
FCS Planning	14256	15552	12960
V2G Implementation	0	1944	1555
Total	67895	58441	68058
Load Shedding (MWh)	2.8241	1.2509	0.0232

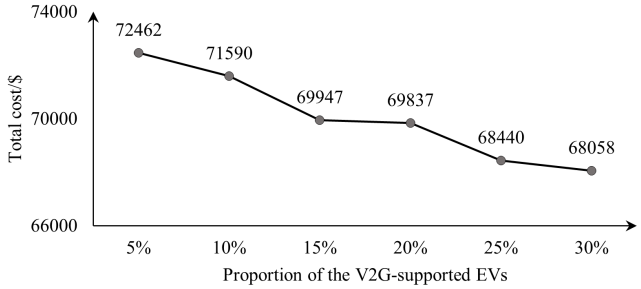

Fig. 8: Total cost considering the flexibility of supported EVs.

implementation planning is lower than that in Case 7, indicating a clear influence of traffic flow uncertainty on the coupled network planning. Furthermore, when comparing the total cost of Case 6 and Case 8, it suggests that with the proposed planning method, the total costs are nearly identical, and simultaneously, the total load shedding can be maintained at a very low level even in the worst situations.

3) Sensitivity Analysis: Furthermore, a sensitivity analysis regarding the proportion of EVs participating in V2G is conducted and illustrated in Fig. 8. The maximum proportion of supported EVs ranges from 5% to 30%. As the proportion increases, the total cost decreases from $72,462 to $68,058, highlighting a strong correlation between the number of EVs engaging in grid support and the total cost. Consequently, under contingency situations, planners can encourage more vehicles to participate in V2G by offering higher additional V2G fees, simultaneously reducing the total cost.

VI. CONCLUSION

This paper provides a robust resilient planning approach for the integrated PDN and TN by taking into account EVs re-dispatching and V2G support. The model integrates the uncertainty associated with traffic flow and the number of EVs participating in V2G, transforming the optimization problem into a two-stage framework. In the first stage, the planning encompasses the reinforcement and expansion of electric lines, the location of FCSs, and V2G modules. The second stage addresses the operational aspect, incorporating the uncertainties in traffic flow and fault scenarios. Additionally, an incentive fee for grid-supported EVs is factored in to ensure driver willingness to support the PDN. In essence, this model provides a comprehensive solution for both the planning of the integrated network and the coordination of vehicle dispatch.

The proposed method has been evaluated by Matlab platform with embedded Gurobi. Simulation results demonstrate that when V2G participates in grid support during contingency situations without uncertain traffic demand, there is a substantial reduction in the total cost compared to scenarios without V2G. Moreover, if uncertain traffic demands are also considered, the proposed robust resilient planning will also be an effective solution within reasonable investment plans.

Currently, the fluctuations in the State of Charge (SOC) of EVs have not been thoroughly addressed. In our forthcoming research, we plan to take into account EVs with different SOC levels and investigate their impact on the proposed resilience enhancement plan. Hopefully, more progress will be reported soon.

APPENDIX A
CONNECTION WITH THE TWO-STAGES MODEL AND THE ROBUST MODEL IN (50)

To elucidate variables in (50) and establish their connection with variables of the two-stages model in Sec. III, this appendix provides a detailed description of variables in (50).

- $M_{n,t}$: the uncertainties of variables in the two-stages model, specifically the traffic flow of EVA (TA^r), EVB (TB^r), and VC (TC^r) in this study.
- $\boldsymbol{C}$: the continuous variables in the first stage model (7)-(9).
- $\boldsymbol{Z}$: the binary variables in the first stage model (7)-(9), encompassing the investment in electric line expansion and hardening, FLC implementation, and V2G equipment implementation.
- $\boldsymbol{U}$: the binary variables in the second stage model (10)-(44) excluding $\boldsymbol{Z}$.
- $\boldsymbol{D}$: the continuous variables in the second stage model (10)-(44) excluding $\boldsymbol{C}$.
- $\boldsymbol{\phi}$: the coefficient matrix of $\boldsymbol{C}$ in the first stage model (7)-(9).
- $\boldsymbol{\varphi}$: the coefficient matrix of $\boldsymbol{Z}$ in the first stage model (7)-(9).
- $\boldsymbol{\kappa}$: the coefficient matrix of $\boldsymbol{C}$ in the second stage model (10)-(44).
- $\boldsymbol{\lambda}$: to the coefficient matrix of $\boldsymbol{Z}$ in the second stage model (10)-(44).
- $\boldsymbol{\theta}$: the coefficient matrix of $\boldsymbol{U}$ in the second stage model (10)-(44).
- $\boldsymbol{\vartheta}$: the coefficient matrix of $\boldsymbol{D}$ in the second stage model (10)-(44).

APPENDIX B
ROAD CAPACITY OF TN UNDER NATURAL DISASTERS

During a natural disaster event, the TN may experience disruptions, leading to a decrease in the capacity of each road. The adjusted road capacity, accounting for road damage, can be expressed as follows:

$$t_a = t_a^0 \left[1 + 0.15 \left(\frac{m_a}{c_a^1}\right)^4\right], \tag{56}$$

$$c_a^1 = (1 - u_a)\, \rho c_a^0 + u_a c_a^0, \tag{57}$$

where c_a^1 is the new road capacity in the congestion state, ρ is the reduction coefficient of road capacity, and u_a is a binary variable to indicate the state of the road which is influenced by the natural disasters. To deal with the nonlinear item $(\frac{1}{c_a^1})^4$ in (56), the linearization process is shown in (58):

$$t_a = t_a^0 + u_a \frac{0.15 m^{aux} t_a^0}{\left(c_a^0\right)^4} + (1 - u_a) \frac{0.15 m^{aux} t_a^0}{\left(\rho c_a^0\right)^4}, \quad (58)$$

where m^{aux} equals to ${m_a}^4$ and the piecewise linearization method can be implemented to represent m^{aux}.

REFERENCES

[1] Global EV Outlook 2023, Int. Energy Agency, Paris, France, 2023.

[2] M. D. Galus, R. A. Waraich, F. Noembrini, K. Steurs, G. Georges, K. Boulouchos, K.W. Axhausen, and G. Andersson, "Integrating power systems, transport systems and vehicle technology for electric mobility impact assessment and efficient control," *IEEE Trans. Smart Grid*, vol. 3, no. 2, pp. 934–949, June 2012.

[3] Y. Wang, J. Shi, R. Wang, Z. Liu, and L. Wang, "Siting and sizing of fast charging stations in highway network with budget constraint," *Appl. Energy*, vol. 228, pp. 1255–1271, Oct. 2018

[4] S. N. Hashemian, M. A. Latify, and G. R. Yousefi, "PEV fast-charging station sizing and placement in coupled transportation-distribution networks considering power line conditioning capability," *IEEE Trans. Smart Grid*, vol. 11, no. 6, pp. 4773-4783, Nov. 2020

[5] L. Geng, Z. Lu, L. He, J. Zhang, X. Li, and X. Guo, "Smart charging management system for electric vehicles in coupled transportation and power distribution systems", *Energy*, vol. 189, no. 116275, 2019.

[6] S. Xie, Z. Hu and J. Wang "Scenario-based comprehensive expansion planning model for a coupled transportation and active distribution system", *Applied Energy*, vol. 255, no. 113782, 2019.

[7] C. Li, Z. Dong, G. Chen, B. Zhou, J. Zhang, and X. Yu, "Data-driven planning of electric vehicle charging infrastructure: a case study of Sydney, Australia", *IEEE Trans. Smart Grid*, vol. 12, no. 4, pp. 3289-3304, Jul. 2021.

[8] W. Wei, L. Wu, J. Wang, and S. Mei, "Expansion planning of urban electrified transportation networks: a mixed-integer convex programming approach", *IEEE Tran. Transportation Electrification*, vol. 3, no. 1, pp. 210-224, Mar. 2017.

[9] H. Zhang, S. J. Moura, Z. Hu, W. Qi, and Y. Song, "A second-order cone programming model for planning PEV fast-charging stations", *IEEE Trans. Power Systems*, vol. 33, no. 3, pp. 2763-2777, May. 2018.

[10] Z. Zhao, C. K. M. Lee, J. Ren and Y. P. Tsang, "Optimal EV fast charging station deployment based on a reinforcement learning framework," *IEEE Trans. Intelligent Transportation Systems*, vol. 24, no. 8, pp. 8053-8065, Aug. 2023.

[11] X. Wang, M. Shahidehpour, C. Jiang and Z. Li, "Coordinated planning strategy for electric vehicle charging stations and coupled traffic-electric networks", *IEEE Trans. Power Systems*, vol. 34, no. 1, pp. 268-279, Jan. 2019.

[12] Y. Sun, P. Zhao, L. Wang L, and S. M. Malik, "Spatial and temporal modelling of coupled power and transportation systems: A comprehensive review", *Energy Conversion and Economics*, vol. 2, no. 2, pp. 55-66, 2021.

[13] W. Wu, Y. Lin, R. Liu, W. Jin, "The multi-depot electric vehicle scheduling problem with power grid characteristics", *Transportation Research Part B: Methodological*, Vol. 155, pp. 322-347, Jan. 2022.

[14] Y. Lin, K. Zhang, Z. J. M. Shen, et al. "Multistage large-scale charging station planning for electric buses considering transportation network and power grid". *Transportation Research Part C: Emerging Technologies*, vol. 107, pp. 423-443, 2019.

[15] T. Qian, C. Shao, X. Li, X. Wang, and M. Shahidehpour, "Enhanced coordinated operations of electric power and transportation networks via EV charging services", *IEEE Trans. Smart Grid*, vol. 11, no. 4, pp. 3019-3030, July 2020.

[16] Y. Sun, Z. Chen, Z. Li, W. Tian, and M. Shahidehpour, "EV charging schedule in coupled constrained networks of transportation and power system", *IEEE Trans. Smart Grid*, vol. 10, no. 5, pp. 4706-4716, Sept. 2019.

[17] Y. Ding, S. Li, S. Jian, "Optimal pricing and fleet management for shared electric vehicle in coupled power and transport networks", *Transportation Research Part C: Emerging Technologies*, Vol. 141, 103727, 2022.

[18] Y. Zhou, Q. Meng, G. P. Ong, "Electric bus charging scheduling for a single public transport route considering nonlinear charging profile and battery degradation effect". *Transportation Research Part B: Methodological*, vol. 159, pp. 49-75, 2022.

[19] A. M. Salman, Y. Li, and M. G. Stewart, "Evaluating system reliability and targeted hardening strategies of power distribution systems subjected to hurricanes," *Rel. Eng. Syst. Saf.*, vol. 144, pp. 319–333, Dec. 2015.

[20] U.S. Government Accountability Office, "Electricity grid resilience: climate change is expected to have far-reaching effects and DOE and FERC should take actions," Mar. 2021. https://www.gao.gov/products/gao-21-346

[21] M. Panteli, D. N. Trakas, P. Mancarella, and N. D. Hatziargyriou, "Power systems resilience assessment: hardening and smart operational enhancement strategies," *Pro. of IEEE*, vol. 105, no. 7, pp. 1202-1213, July 2017.

[22] S. Ma, B. Chen, and Z. Wang, "Resilience enhancement strategy for distribution systems under extreme weather events," *IEEE Trans. Smart Grid*, vol. 9, no. 2, pp. 1442–1451, Mar. 2018.

[23] T. Ding, Z. Wang, W. Jia, B. Chen, C. Chen, and M. Shahidehpour, "Multiperiod distribution system restoration with routing repair crews, mobile electric vehicles, and soft-open-point networked microgrids," *IEEE Trans. Smart Grid*, vol. 11, no. 6, pp. 4795–4808, Nov. 2020.

[24] M. E. Khodayar, L. Wu, and Z. Li, "Electric vehicle mobility in transmission-constrained hourly power generation scheduling," *IEEE Trans. Smart Grid*, vol. 4, no. 2, pp. 779–788, Jun. 2013.

[25] S. Liu, C. Chen, Y. Jiang, Z. Lin, H. Wang, M.Waseem, and F. Wen, "Bi-level coordinated power system restoration model considering the support of multiple flexible resources," *IEEE Trans. Power Systems*, vol. 38, no. 2, pp. 1583-1595, March 2023.

[26] C. Shao, T. Qian, Y. Wang and X. Wang, "Coordinated planning of extreme fast charging stations and power distribution networks considering on-site storage", *IEEE Trans. Intelligent Transportation Systems*, vol. 22, no. 1, pp. 493-504, Jan. 2021.

[27] J. Hu, C. Ye, Y. Ding, J. Tang, and S. Liu, "A distributed MPC to exploit reactive power V2G for real-time voltage regulation in distribution networks," *IEEE Trans. Smart Grid*, vol. 13, no. 1, pp. 576-588, Jan. 2022.

[28] N. Liu, X. Hu, L. Ma, and X. Yu, "Vulnerability assessment for coupled network consisting of power grid and EV traffic network," *IEEE Trans. Smart Grid*, vol. 13, no. 1, pp. 589-598, Jan. 2022.

[29] M. R. Sarker, Y. Dvorkin, and M. A. Ortega-Vazquez, "Optimal participation of an electric vehicle aggregator in day-ahead energy and reserve markets," *IEEE Trans. Power Syst.*, vol. 31, no. 5, pp. 3506–3515, Sept. 2016.

[30] A. S. Debs, *Modern Power Systems Control and Operation*, Kluwer Academic Publishers, 1988.

[31] W. Gan, M. Shahidehpour, J. Guo, W. Yao, A. Paaso, L. Zhang, and Jinyu Wen, "Two-stage planning of network-constrained hybrid energy supply stations for electric and natural gas vehicles", *IEEE Trans. Smart Grid*, vol. 12, no. 3, pp. 2013–2026, May 2021.

[32] M. Yan, X. Ai, M. Shahidehpour, Z. Li, J. Wen, S. Bahramira, and A. Paaso, "Enhancing the transmission grid resilience in ice storms by optimal coordination of power system schedule with prepositioning and routing of mobile DC deicing devices," *IEEE Trans. Power Syst.*, vol. 34, no. 4, pp. 2663–2674, Jul. 2019.

[33] W. Wei and J. Wang, *Modeling and Optimization of Interdependent Energy Infrastructures*, Springer Nature, Switzerland, AG, 2020.

[34] X. A. Sun and A. J. Conejo, *Robust Optimization in Electric Energy Systems*, Int. Series in Operations Research & Management Science, Vol, 313, Springer Nature, Switzerland AG, 2021.

[35] B. Zeng, and L. Zhao, "Solving two-stage robust optimization problems using a column-and-constraint generation method," *Operations Research Letters*, vol. 41, no. 5, pp. 457-461, 2013.

[36] H. Hajian-Hoseinabadi, "Impacts of automated control systems on substation reliability," *IEEE Trans. Power Delivery*, vol. 26, no. 3, pp. 1681-1691, July 2011.

[37] W. Li, J. Zhou, J. Lu, and W. Yan, "A probabilistic analysis approach to making decision on retirement of aged equipment in transmission systems," *IEEE Trans. Power Delivery*, vol. 22, no. 3, pp. 1891-1896, July 2007.

[38] J.-F. Moon, J.-C. Kim, H.-T. Lee, C.-H. Park, S.-Y. Yun, and S.-S. Lee, "Reliability evaluation of distribution system through the analysis of time-varying failure rate," *IEEE Power Engineering Society General Meeting*, 2004., Denver, CO, USA, 2004, pp. 668-673 Vol.1

[39] C. Ali and D. Koval. *Power Distribution System Reliability: Practical Methods and Applications*, John Wiley & Sons, 2011.

[40] W. Gan, M. Shahidehpour, J. Guo, W. Yao, S. Pandey, E. A. Paaso, A. Vukojevic, and J. Wen, "A tri-level planning approach to resilient expansion and hardening of coupled power distribution and transportation systems," *IEEE Trans. Power Systems*, vol. 37, no. 2, pp. 1495-1507, March 2022.
[41] C. Zhang, Z. Dong and L. Yang, "A feasibility pump based solution algorithm for two-stage robust optimization with integer recourses of energy storage systems," *IEEE Trans. Sustainable Energy*, vol. 12, no. 3, pp. 1834-1837, July 2021.
[42] H. Gao, J. Liu and L. Wang, "Robust coordinated optimization of active and reactive power in active distribution systems," *IEEE Trans. Smart Grid*, vol. 9, no. 5, pp. 4436-4447, Sept. 2018.

Jianfeng Wen (Student Member, IEEE) received the B.S. and M.Eng. degrees in electrical engineering from the Huazhong University of Science and Technology, Wuhan, China, in 2018 and 2020, respectively. He is currently working toward the Ph.D. degree as a dual Ph.D. Student in electrical engineering with The University of Liverpool, Liverpool, U.K., and National Tsing Hua University, Hsinchu, Taiwan. His research interests include control and energy management of micro-grid systems, and electrified transportation optimization.

Chia-Chi Chu (M'96–SM'15) received B.S. and M.S. degrees from National Taiwan University, Taipei, Taiwan, in 1987 and 1989 respectively, and a Ph.D. from Cornell University, Ithaca, NY, USA, in 1996, all in electrical engineering. From 1995 to 1996, he was a member of the Technical Staff at Avant! Corporation, Fremont, CA, USA. From 1996 to 2006, he was a faculty member of electrical engineering at Chang Gung University, Taoyuan, Taiwan. He was a visiting scholar at the University of California at Berkeley, Berkeley, CA, USA, and the University of Sydney, Sydney, NSW, Australia, Nanyang Technological University, Singapore, in 1999, 2014, and 2019 respectively. Since 2006, he has been a faculty member of electrical engineering at National Tsing Hua University, Hsinchu, Taiwan, and is currently a professor. His current research interests include power system stability and microgrid control.

Dr. Chu was the recipient of the Outstanding Research Award from the Ministry of Science and Technology (MOST), Taiwan, in 2020, Outstanding Professor of Electrical Engineering Award from the Chinese Institute of Electrical Engineering, Taiwan, 2021, the Young Author Award from IEEE Control of Oscillations and Chaos Conference (COC) in 1997, the Best Paper Awards from IEEE 8th International Conference on Power Electronics and Drive Systems (PEDS) in 2009, the Best Paper Awards from IEEE 4th International Future Energy Electronics Conference (IFEEC) in 2019, and the Second Prize Award from Industrial Automation and Control Committee, *IEEE Industry Applications Society* in 2021. From 2015 to 2017, he was the Chair of the Power and Energy Circuits and Systems Technical Committee of the IEEE Circuits and Systems Society. He was the Chairman of IEEE Power Engineering Society (PE-31), Taipei Section from 2019 to 2021, and an Associate Editor of *IEEE Trans. Power Systems* from 2019 to 2023. Currently, he is the director of IEEE Taipei Section, and an Associate Editor of *IEEE Trans. Ind. Appl.* , *Int. Trans. Electrical Energy Systems*, and *Int. J. Electrical Engineering*.

Wei Gan (Member, IEEE) received the B.S. and Ph.D. degrees in electrical engineering from the Huazhong University of Science and Technology, Wuhan, China, in 2016 and 2021, respectively. From 2018 to 2019, he was a Visiting Ph.D. Student with the China Electric Power Research Institute, Beijing, China. From 2019 to 2020, he was a Visiting Ph.D. Student with the Robert W. Galvin Center for Electricity Innovation, Illinois Institute of Technology, Chicago, IL, USA. He is currently a Postdoctoral Research Associate with the School of Engineering, Cardiff University, Cardiff, U.K. His research interests include peer-to-peer energy trading, coordinated optimization of power-traffic systems, and multiple energy system integration.

Lin Jiang (Member, IEEE) received the B.Sc. and M.Sc. degrees from the Huazhong University of Science and Technology, Wuhan, China, and the Ph.D. degree from the University of Liverpool, Liverpool, U.K., in 1992, 1996, and 2001, respectively, all in electrical engineering. He was a Postdoctoral Research Assistant with the University of Liverpool from 2001 to 2003 and a Postdoctoral Research Associate with the Department of Automatic Control and Systems Engineering, University of Sheffield, Sheffield, U.K., from 2003 to 2005. He was a Senior Lecturer with the University of Glamorgan, Wales, U.K., from 2005 to 2007, and joined the University of Liverpool in 2007. He is currently a Reader with the Department of Electrical Engineering and Electronics, University of Liverpool, U.K. His current research interests include control and analysis of power system, smart grid, renewable energy and power electronics.

Jiajie Luo received the B.Eng. degree from the Huazhong University of Science and Technology, Wuhan, China and the University of Birmingham, Birmingham, U.K., in 2015. And he received the Ph.D. degree in electrical engineering from the University of Birmingham, in 2019. He is currently a senior engineer at Arup, UK. His research interests include renewable energy integration, modeling, and control.